Structural and evolutionary characteristics of dynamin-related GTPase OPA1

Dandan Li [1, 2], **Jinlan Wang** [3], **Zichen Jin** [4], **Zheng Zhang** [Corresp. 5]

[1] College of Biological Sciences, China Agricultural University, Beijing, China

[2] National Institute of Biological Sciences, Beijing, China

[3] Physical Examination Office of Shandong Province, Health Commission of Shandong Province, Jinan, China

[4] Department of Chemistry, University of Minnesota, Minnesota, USA

[5] State Key Laboratory of Microbial Technology, Institute of Microbial Technology, Shandong University, Qingdao, China

Corresponding Author: Zheng Zhang
Email address: zhangzheng@sdu.edu.cn

OPA1 is a dynamin-related GTPase that controls mitochondrial fusion, cristae remodeling, energetics and mtDNA maintenance. However, the molecular architecture of OPA1 is poorly understood. Here we modeled the structure of human OPA1 by the threading approach. We found that the C-terminal region of the OPA1 protein had multiple functional domains, while the N-terminal region was rich in alpha helices and did not include specific domains. For the short soluble forms of OPA1, we observed that there were obvious hydrophobic regions near the two cleavage sites and the N-terminal was positively charged after cleavage. The blue native analysis revealed that the protein could form stable homodimers. In addition, the evolutionary conservation of the C-terminal region, where most of the known mutated disease-related sites were located in, was significantly higher than that of the N-terminal region. These findings provided new insights into the structure and biochemical function of OPA1.

Structural and evolutionary characteristics of dynamin-related GTPase OPA1

Dandan Li [1,2], Jinlan Wang [3], Zichen Jin [4] and Zheng Zhang [5*]

[1]College of Biological Sciences, China Agricultural University, Beijing 100083, China.

[2]National Institute of Biological Sciences, Beijing 102206, China.

[3]Physical Examination Office of Shandong Province, Health Commission of Shandong Province, Jinan 250014, China.

[4]Department of Chemistry, University of Minnesota, Minnesota 55455, USA.

[5]State Key Laboratory of Microbial Technology, Institute of Microbial Technology, Shandong University, Qingdao 266237, China.

* The corresponding author.

Email addresses of the authors:

Dandan Li, lidandan@nibs.ac.cn

Jinlan Wang, jinlan726@163.com

Zichen Jin, jinxx631@umn.edu

Zheng Zhang, zhangzheng@sdu.edu.cn

Abstract

OPA1 is a dynamin-related GTPase that controls mitochondrial fusion, cristae remodeling, energetics and mtDNA maintenance. However, the molecular architecture of OPA1 is poorly understood. Here we modeled the structure of human OPA1 by the threading approach. We found that the C-terminal region of the OPA1 protein had multiple functional domains, while the N-terminal region was rich in alpha helices and did not include specific domains. For the short soluble forms of OPA1, we observed that there were obvious hydrophobic regions near the two cleavage sites and the N-terminal was positively charged after cleavage. The blue native analysis revealed that the protein could form stable homodimers. In addition, the evolutionary conservation of the C-terminal region, where most of the known mutated disease-related sites were located in, was significantly higher than that of the N-terminal region. These findings provided new insights into the structure and biochemical function of OPA1.

Introduction

Mitochondria undergo a constant dynamic balance between organelles fusion and fission to maintain their network morphology and functions (van der Bliek et al. 2013; Wai & Langer 2016). The functional relevance of mitochondrial dynamics has been emphasized by its requirement during embryonic development and its repercussions in the main functions of the organelle, including respiration, response to cellular stress, calcium homeostasis and apoptosis (Chan 2012; Eisner et al. 2018; Noguchi & Kasahara 2018). Several conserved GTPase mediate the mitochondrial dynamics: mitofusins (mitofusin 1 and mitofusin 2) control fusion of the outer mitochondrial membrane (OMM) while Drp1 is involved in fission of OMM (Labbe et al. 2014; Pernas & Scorrano 2016); the conserved dynamin-related GTPase optic atrophy 1 (OPA1) is indispensable for both cristae morphology and the inner mitochondrial membrane (IMM) fusion (Belenguer & Pellegrini 2013; Del Dotto et al. 2018a; Pernas & Scorrano 2016).

Many evidences indicate that OPA1 is associated with other important mitochondrial functions, including mitochondrial DNA (mtDNA) maintenance, which is probably anchored to the IMM, and the oxidative phosphorylation efficiency (Belenguer & Pellegrini 2013; Del Dotto et al. 2018a). In mouse embryonic fibroblasts, global loss of OPA1 results in fragmentation of the mitochondrial network, together with critically reduced mtDNA copy number, as well as significant disorganization of cristae structure and a reduction of respiratory capacity (Chen et al. 2010; Cogliati et al. 2013; Song et al. 2007; Song et al. 2009). Re-expression of any OPA1 isoform can restore energetic efficiency, mtDNA content, and cristae structure (Del Dotto et al.

2017). OPA1 oligomerization, tightening cristae junctions, is required for apoptosis regulation by maintaining the cytochrome c inside the cristae and controlling its release (Frezza et al. 2006; Olichon et al. 2003; Yamaguchi et al. 2008). In addition, OPA1-dependent modulation of cristae structure is necessary for cellular adaptation to energy substrate availability (Patten et al. 2014).

Mutations in *OPA1* cause the disease dominant optic atrophy (DOA), one inherited optic neuropathy that is characterized by selective degeneration of retinal ganglion cells and classically presents in early childhood with progressive visual failure (Del Dotto et al. 2018b; Lenaers et al. 2012). Biochemical studies indicated that OPA1 disease alleles associated with DOA displayed a variety of mitochondrial defects in several activities, involving GTP hydrolysis, cardiolipin association, and membrane tubulation (Ban et al. 2010; Belenguer & Pellegrini 2013; Zanna et al. 2008). Compared with the classical optic atrophy, DOA and deafness (DOAD) associating neurosensory deafness and DOA plus involving in other clinical manifestations like myopathy, progressive external ophthalmoplegia or spastic paraplegia, are syndromic dominant optic atrophy (Amati-Bonneau et al. 2008; Del Dotto et al. 2018b; Lenaers et al. 2012; Yu-Wai-Man et al. 2010). Moreover, *OPA1* mutations have been related to an expanding spectrum of neurodegenerative phenotypes, such as Behr-like syndrome, syndromic parkinsonism, dementia and others (Carelli et al. 2015; Del Dotto et al. 2018b; Marelli et al. 2011).

OPA1 belongs to the dynamin superfamily proteins. Dynamins are large GTPases, including classical dynamins (dynamin 1, dynamin 2, dynamin 3), mitofusins, Drp1, OPA1, Mx proteins, guanylate-binding proteins (GBPs) and atlastins in eukaryotic cells (Jimah & Hinshaw

2019). The mitofusins, Drp1, OPA1 and atlastins are involved in the process of membrane remodeling; the classical dynamins mainly function in the clathrin-mediated endocytosis and budding of vesicles; additional dynamins like GBPs and Mx proteins restrict pathogens (Anderson et al. 1999; Haller et al. 1981; Pernas & Scorrano 2016). Several structures of dynamins have been solved so far (Jimah & Hinshaw 2019). The structures show that all dynamins include a GTPase domain that binds and hydrolyzes GTP and an α-helical bundle domain. Most of dynamins also contain a middle domain involved in oligomerization and a GTPase effector domain (GED) that are associated with stimulation of GTPase activity. Several dynamins contain a domain that can be a transmembrane domain, a sequence or a pleckstrin-homology domain (PH domain) for interacting with lipid membranes (Praefcke & McMahon 2004). However, due to its exceptional complexity there is still no crystal structure of OPA1 protein.

In human, the *OPA1* gene is built from 30 exons and has been reported to generate at least eight mRNA variants by the alternative splicing of exons 4, 4b and 5b (Fig. 1A). OPA1 is a dynamin-related GTPase with a mitochondrial targeting sequence (MTS), followed by a transmembrane (TM), which need to be further cleaved to execute mitochondrial function (Belenguer & Pellegrini 2013). Precursors translated from the eight OPA1 mRNA are targeted to mitochondria via MTS, which is cleaved by the mitochondrial processing peptidase (MPP) to give rise to the long forms (l-forms) anchored to IMM. About half of l-forms are then further proteolytically processed by OMA1 and YME1L proteases to produce the short forms (s-forms),

which are soluble in the mitochondrial intermembrane space (IMS) (Anand et al. 2014; Ishihara et al. 2006; MacVicar & Langer 2016; Song et al. 2007). Remarkably, the four isoforms including exon 4b are completely processed into s-forms (Song et al. 2007). Although OPA1 protein have been studied for many years, the molecular architecture of OPA1 must be elucidated to better understand its functions. Here, we modeled the structure of the human OPA1 by the threading approach, analyzed the protein-protein interaction, and explored the characteristics of the sequences and structures through bioinformatics analysis.

Materials & Methods

OPA1 information acquisition

The information of human *OPA1* gene, exons and isoforms were obtained from the NCBI and Ensemble databases (Zerbino et al. 2018). The other vertebrate OPA1 protein sequences were acquired from the NCBI reference sequence (RefSeq) database (O'Leary et al. 2016). All partial sequences and low quality proteins were excluded. The crystal structures of proteins from dynamin family were obtained from the PDB database (Rose et al. 2017).

Sequence analysis

The theoretical isoelectric points and the grand average hydropathicity were calculated by ExPASy server (Bjellqvist et al. 1993). The eight human OPA1 isoforms and all vertebrates OPA1 proteins were aligned with MAFFT (Katoh & Standley 2013), respectively. Using the

113 longest splice variant OPA1 in vertebrates, the evolutionary conservations of amino acid residue
114 positions in the OPA1 sequences was measured by using ConSurf algorithm (Ashkenazy et al.
115 2016). The best evolutionary substitution model was used and calculation was based on the
116 Empirical Bayesian paradigm. The sequence and modeled structure of human OPA1 were used
117 to show the nine-color conservation grades. Sequence logos were generated as graphical
118 representations of the multiple sequence alignments of the amino acids (Crooks et al. 2004).
119 Phylogenetic analyses were conducted using MEGA version 7 by the bootstrap neighbor joining
120 method (Kumar et al. 2016).

121 **Structural analysis**

122 I-TASSER was used to predict the structures of the human OPA1 protein (Yang et al. 2015).
123 The structural model was refined by fragment-guided molecular dynamics (FG-MD) simulations
124 at the atomic-level (Zhang et al. 2011). The quality assessment of Ramachandran plot had been
125 used to quantitatively assess the accuracy of protein structure predictions. The statistical data of
126 Ramachandran plot was calculated by PROCHECK (Laskowski et al. 1993). The protein
127 structures were displayed by PyMol (Schrödinger, LLC). Pairwise structural differences between
128 human OPA1 and other proteins from dynamin family were measured by TM-align (Zhang &
129 Skolnick 2005). The structural similarity of two protein structures was measured with the TM-
130 score that had the value (0, 1) (Xu & Zhang 2010). The higher the value was, the more similar
131 the two aligned structures were. The two modeled structures of human OPA1 protein were taken
132 as target 1 and target 2, respectively, to submit to PRISM protein–protein docking server for

133 predicting possible interactions and how the interaction partners structurally connect (Baspinar et
134 al. 2014).

135 **Protein purification and blue native page**

136 A human *OPA1* construct (exons 6-28) was expressed in *Escherichia coli* BL21 (DE3) cells
137 as N-terminal His_6-SUMO-tagged fusion proteins using the pET28a plasmid (His_6-SUMO-
138 OPA1). Cells were grown in LB medium at 37 °C to an OD_{600} of ~0.6. Protein expression was
139 induced by addition of 100 μM IPTG and cultures were incubated overnight at 16 °C. The cell
140 pellet was resuspended in 10 mM Tris-HCl pH 8.0, 20 mM imidazole and 500 mM NaCl buffer.
141 Cells were lysed using a microfluidizer (Microfluidics). After centrifugation at 12,000 rpm for 1
142 h at 4 °C, the soluble extract was filtered and combined with Ni-NTA agarose (GE Healthcare)
143 in batch. After beads were packed into a column, the combination was washed with resuspension
144 buffer supplemented with 40 mM imidazole, and protein was eluted with an imidazole gradient
145 to a final concentration of 500 mM. Peak fractions were pooled, and the His_6-SUMO-tag was
146 cleaved by ULP1 peptidase in the 4 °C overnight to generate the OPA1 (exons 6-28) protein.
147 Then diluted the NaCl concentration to 50 mM and applied to Resource Q column (GE
148 Healthcare). Peak fractions were concentrated and loaded to a Superdex 200 10/300 gel filtration
149 column (GE Healthcare) using the buffer with 10 mM Tris-HCl, pH 8.0 and 150 mM NaCl. The
150 protein was concentrated to ~10 mg/ml prior to freezing. All the samples were analyzed by SDS-
151 PAGE electrophoresis. The procedure for SDS-PAGE was based on a general protocol as
152 previously described (Simpson 2006). All the samples heated at 95℃ for 10 min and loaded onto

153 a polyacrylamide gel that was consist of 5% stacking and 10% resolving gel, which was run at 80
154 V for 0.5 h, and then at 100 V for 1 h.

155 Blue native page was performed as described previously with slight modifications (Wittig et
156 al. 2006). 10 mg of the OPA1 (exons 6-28) protein was loaded into a blue native page gel that
157 was consist of 3.5% stacking and 4–10% gradient separating gel. The cathode buffer (7.5 mM
158 imidazole with pH 7.0, 50 mM tricine, supplemented with 0.02% w/v coomassie brilliant blue
159 G250) and the anode (25 mM imidazole with pH 7.0) were chilled at 4 °C before used. Then,
160 electrophoresis was started at 80 V for 30 min and adjusted to 120 V for 10 h.

161

162 Results

163 Sequence analysis of human OPA1 isoforms

164 The human *OPA1* gene contains eight spliced variants (Fig. 1A). Proteolytically processed
165 by OMA1 and YME1L proteases in the domains were corresponding to exons 5 and 5b,
166 containing the cleavage sites S1 and S2, respectively. In principle, each mRNA variant form can
167 produce a long isoform and one or more short isoforms. However, the four isoforms (3, 5, 6 ,8)
168 including exon 4b completely processed into s-forms. We confirmed that exon 4b-encoded
169 peptide was hydrophobic while the others around were hydrophilic (Fig. 1B), which was
170 consistent with the previous study (Elachouri et al. 2011). The hydrophobicity of exon 4b-
171 encoded peptide might be helpful to recruit the OMA1 protease, thus, promoting the cleavage at

site S1. Although exon 5b-encoded peptide was hydrophilic as a whole, there was a hydrophobic region just before site S2, hypothesizing that the hydrophobic segment can associate with YME1L protease to promote the cleavage at site S2.

We also noticed that the N-terminus of OPA1 s-forms were positively charged (Fig. 1C). The isoelectric point (pI) value of exon 5-encoded peptide was 6.8, while the pI value of the remaining peptide segment increased to 8.6 after being cleaved at site S1. Similarly, the pI value of exon 5b-encoded peptide rose from 6.8 to 9.5 after the site S2 was cut. This result revealed that the N-terminal of OPA1 s-forms all had positive charge no matter it was cleaved at site S1 or S2.

Structure characteristic of human OPA1

Taking the longest splice variant 8 including 30 exons as an example, we used the threading approach to model the three-dimensional structure of human OPA1 protein excluding MTS and TM regions (Fig. 2). According to quality assessment, the accuracy of the OPA1 protein structural models were acceptable (Fig. S1). The structure showed that OPA1 protein could be clearly divided into two regions, the N-terminal and C-terminal region. The N-terminal region (encoded by exons 3-8) was rich in alpha helix, which did not include specific domains. The difference among the 8 spliced variants of OPA1 protein, l-forms and s-forms was the region of N-terminal. The N-terminal region of l-forms contained 138-228 amino acid residues, while s-forms included only 104-134 residues.

192 The C-terminal region of OPA1 protein was a dense structure containing multiple domains
193 and was identical for all isoforms. In the human OPA1 protein, each domain of the C-terminal
194 region had perfectly corresponded with exons. The GTPase domain corresponded with exons 9-
195 16, middle domain corresponded with exons 19-22 and a GED corresponded with exons 26-
196 28. The peptide encoded by exons 17-18 formed a long helix that connected GTPase domain and
197 middle domain. The exons 23-25 encoded a peptide, a PH domain, located between middle
198 domain and GED.

199 The PH domain of classical dynamins is responsible for their interaction with negatively
200 charged lipid membranes (Praefcke & McMahon 2004). The pI analysis indicated that the pI
201 value of PH domain of human OPA1 protein was 7.7, especially the pI value of exon 25-encoded
202 peptide was as high as 9.5 whereas the pI value of the middle domain and GED next to PH
203 domain were 5.0 and 6.8, respectively. Thus, the PH domain of OPA1 carried positive charge,
204 might be involved in interaction with negatively charged phospholipid molecules.

205 Comparing the structure of the C-terminal region of human OPA1 protein with the nine-
206 known structures of the dynamin superfamily proteins (Fig. 3), the results showed that OPA1 and
207 other human dynamins had two common domains: a GTPase domain and an α-helical bundle.
208 Interestingly, human OPA1 protein was similar to dynamin 1, dynamin 3, Drp1, MxA and MxB
209 proteins, and the TM-score of all was higher than 0.5, although these proteins did not mediate
210 membrane fusion like OPA1. Comparing OPA1 with mitofusin 1, atlastin 1 and altastin 3, which
211 were involved in membrane fusion, the TM-score of all was minor than 0.3. In addition, similar

212 to dynamin 1, dynamin 3 and Drp1, OPA1 had a PH domain, while other proteins involved in
213 fusion process did not have. Significant structural differences indicated that OPA1 might have a
214 unique mechanism for controlling inner membrane fusion.

215

216 **Dimerization of human OPA1 protein**

217 To determine the oligomeric form of OPA1, we expressed the common part of the eight
218 spliced variants of human OPA1 (exons 6-28) protein in *E. coli*. The protein was detected by
219 SDS-PAGE electrophoresis (Fig. S2). From the peak position of the OPA1 (exons 6-28) elution
220 profiles of a S200 size-exclusion column, the result indicated that the molecular weight of the
221 protein was about 170 kD, thus, we speculated the protein may exist as dimers in solution.
222 Additionally, in blue native electrophoresis, we found nucleotide-free OPA1 formed stable
223 dimers and multiple oligomers, indicating that the OPA1 molecule itself could be interacted and
224 formed a stable multimer.

225 Further, we predicted the possible mode of dimerization of the C-terminal region by using
226 the human OPA1 protein modeled structure. Protein-protein docking results showed that the C-
227 terminal region of the human OPA1 protein could form two stable homodimers modes. In the
228 first mode of homodimer, the GTPase domains of the two monomers were approximately 130 Å
229 apart, and the dimeric interface involved in 23 pairs of interaction among 15 amino acid sites, 10
230 pairs of which were from the interaction between the linker domain and middle domain, 12 pairs
231 of which were from the interaction between the middle domain and the GED, while one pair of

232 sites was between the two same GED domains (Fig. 4A). In the second homodimer, the GTPase
233 domains of the two monomers were approximately 100 Å apart, and the dimeric interaction
234 interface involved in 33 pairs of interaction among 18 amino acid sites, 17 pairs of which were
235 from the interaction between two middle domains, 12 pairs of which were from the interaction
236 between the middle domain and the GED, and 4 pairs from the interaction between the two GED
237 domains (Fig. 4B). These results indicated that, similar to dynamin 1 and MxA, OPA1 could
238 assemble to dimers and higher-order oligomers via middle domain and GED, which was
239 different from mitofusins that mediated membrane fusion by GTPase domains (Cao et al. 2017).
240 Additionally, interactions between GTPase-GTPase domains had been reported to be essential
241 for the function of dynamins, but our results showed neither of these two dimeric interfaces of
242 nucleotide-free OPA1 proteins involved in the GTPase domain.

243

244 **Conserved sites in OPA1 protein**

245 Furthermore, we collected all the vertebrate OPA1 proteins by sequence similarity search.
246 Totally, more than 900 of OPA1 protein sequences were discovered from 205 species including
247 several spliced variants. The sequence alignments was shown in the form of sequence logo map
248 (Fig. S3). Using the longest spliced variant of OPA1 protein sequence in each species of
249 vertebrates, we analyzed conserved amino acid sites in the OPA1 proteins and displayed them
250 through the modeled structure of the human OPA1 protein (Fig. 5A).

The results showed that the N-terminal region of OPA1 protein was significantly less conservative than the C-terminal region (Fig. 5B). For those sites with the highest conservation (grade 9), the N-terminal region only occupied 27% of all sites and 66% in the C-terminal region. For those sites with the lowest conservation (grade 1), 43% of all sites were in the N-terminal region and 10% in the C-terminal region. Specifically, in the N-terminal region, the exon 4 and exon 5-encoded peptides had the lowest conservation while the peptides encoded by exons 6-8 had a higher conservation. In the C-terminal region, the conservation of the GTPase domain and the linker encoded by exons 17-18 were the highest, while the PH domain was less conservative. These results indicated that the linkers encoded by exons 17-18 and exons 6-8, next to the GTPase domain, may be functionally important. A large swing in the linker during the GTPase cycle might cause the power-stroke that led to fusion. However, being the PH domain less conserved, it was speculated that its function might vary from species to species.

Disease-related sites in human OPA1 protein

Human OPA1 mutations have been associated to a large spectrum of neurodegenerations. 171 amino acid site variants in the human OPA1 had been analyzed by the locus-specific database dedicated to OPA1 (Data S1). The positions of the amino acid sites in human OPA1 protein were in accord with those of spliced variant 8. These variations include substitutions, duplications, deletions and insertions, but do not include synonymous mutations, nonsense mutations, and frameshift mutations. Of the 171 variants, 136 were associated with diseases, 10

were not related to diseases and 25 were variants of unknown significance. About 80% of disease-related variant sites were the highest conservative in the vertebrate OPA1 proteins (grade 9), while only 30% of the variant sites unrelated to disease had the corresponding values. Besides, 60% of variant sites that were not related to diseases had the lowest conservation (grade 1), while less than 10% of disease-related variant sites were the lowest conservative. Therefore, disease-related mutations in the OPA1 protein occurred mainly at sites with highly evolutionary conservation.

The N-terminal region of OPA1 protein occupied 34% of the total length, but the disease-related mutation sites located in this region accounted for only 15% of the total disease-related mutation sites in the OPA1 while the mutations unrelated to diseases in this region occupied 70% of the total mutation sites unrelated to diseases. The disease-related variant sites in the N-terminal region were concentrated in the exons 1-2 coding region (8 variants) and the exons 6-8 coding region (11 variants), while the variant sites unrelated to disease were concentrated on the exons 4, 4b and 5b (5 variants). For the C-terminal region, more than 25% of the sites in the GTPase domain and the linker region encoded by exons 17-18 were found to have disease-related mutations, respectively. And about 20% of sites in the GED were also found to present disease-related variation. Therefore, most of the disease-related mutations in the OPA1 protein were located in the C-terminal region, while in the alternative splicing region, almost no disease-related mutation occurred.

Discussion

OPA1 is a member of dynamin superfamily, which is essential for shaping the cristae morphology and IMM fusion (Belenguer & Pellegrini 2013; Praefcke & McMahon 2004). In human, the OPA1 proteins include soluble s-forms and l-forms containing the TM region. However, there is a lack of understanding of the whole structure of OPA1 and the structural differences among various spliced variants, l-forms and s-forms. In our study, the modeled structure of human OPA1 protein revealed that its structure was divided into N-terminal and C-terminal regions. N-terminal region did not contain the specific domains and was structurally a long peptide chain rich in alpha helices. The length of the long peptide chain in the N-terminal region was the only difference among the eight OPA1 isoforms, while there was no difference in the functional domains. For the OPA1 s-forms, it lacked the TM region and the length of the peptide chain in the N-terminal region was shorten. More interestingly, we found that the N-terminal of exons 5 and 5b encoding peptides were positively charged after cleavage, indicating that OPA1 s-forms may interact with the negatively charged phospholipid molecules in the membrane.

The C-terminal region of OPA1 protein was a dense structure comprising a GTPase domain, a middle domain, a PH domain and a GED. The structure of this region was different from mitofusins and atlastins that mediated membrane fusion, while it was similar to dynamin 1 and MxA. The OPA1 protein contained a PH domain that interacted with phospholipid molecules, while mitofusins and atlastins did not include. In addition, similar to dynamin 1 and MxA, OPA1

could self-assemble to form dimers through the middle domain and GED, while this was also different from mitofusins and atlastins that dimerized by GTPase-GTPase domains. All these findings indicated that OPA1 might have a specific fusion mechanism.

The prior studies indicated that a homotypic OPA1 interaction, tightening cristae junctions, mediated membrane tethering (Ban et al. 2017; Frezza et al. 2006; Olichon et al. 2003). Our modeled structural analysis indicated that the C-terminal region of human OPA1 protein could form stable homodimer. Although the obvious difference between the eight OPA1 isoforms was concentrated on the N-terminal region, all of them maybe adopt the same mode by trans-OPA1 interaction when maintaining the cristae morphology. The OPA1 s-forms could also form a trans-interaction, and its N-terminal might interact with cardiolipin in the membrane. An in vitro membrane fusion assay unveiled that OPA1 l-form on one side of the membrane and cardiolipin on the other side, are the minimal components sufficient and necessary for fusion (Ban et al. 2017; Liu & Chan 2017). According to the electric charge analysis, the PH domain had a strong positive charge region while cardiolipin had a negative charge region. Furthermore, a deletion mutant assay suggested that the domain next to the GTPase domain was necessary for cardiolipin binding (Ban et al. 2017; Del Dotto et al. 2018a). Combined with our work, we speculated that the charge interaction between PH domain and cardiolipin promoted binding and then accelerated double-membrane fusion. In short, these findings could be useful to better understand the biochemical functions of OPA1.

Conclusions

In this work, we modeled the whole structure of human OPA1 protein, revealing that its structure was divided into N-terminal and C-terminal region. The N-terminal region was rich in alpha helices and did not include specific domains. The eight OPA1 spliced variants only differed in the length of the long peptide chain in the N-terminal region but not in the functional domains. By contrast, the C-terminal region of OPA1 protein was a dense structure containing a GTPase domain, a middle domain, a PH domain, and a GED. The structure of the C-terminal region of OPA1 protein was not similar to that of other dynamin superfamily members that mediated membrane fusion, while it was similar to dynamin 1 and MxA, which could self-assembled to form dimers by the middle domain and GED. Additionally, the evolutionary conservation of the C-terminal region was significantly higher than that of the N-terminal region and the known mutated disease-related sites were mostly located in the C-terminal region of OPA1 protein. Overall, these findings provide novel insights into the structural and evolutionary characterizations of OPA1.

Acknowledgements

We acknowledge Professor Xiangshu Jin of Michigan State University for insight advices on biochemical assays.

References

Amati-Bonneau P, Valentino ML, Reynier P, Gallardo ME, Bornstein B, Boissiere A, Campos Y, Rivera H, de la Aleja JG, Carroccia R, Iommarini L, Labauge P, Figarella-Branger D, Marcorelles P, Furby A, Beauvais K, Letournel F, Liguori R, La Morgia C, Montagna P, Liguori M, Zanna C, Rugolo M, Cossarizza A, Wissinger B, Verny C, Schwarzenbacher R, Martin MA, Arenas J, Ayuso C, Garesse R, Lenaers G, Bonneau D, and Carelli V. 2008. OPA1 mutations induce mitochondrial DNA instability and optic atrophy 'plus' phenotypes. *Brain* 131:338-351. 10.1093/brain/awm298

Anand R, Wai T, Baker MJ, Kladt N, Schauss AC, Rugarli E, and Langer T. 2014. The i-AAA protease YME1L and OMA1 cleave OPA1 to balance mitochondrial fusion and fission. *J Cell Biol* 204:919-929. 10.1083/jcb.201308006

Anderson SL, Carton JM, Lou J, Xing L, and Rubin BY. 1999. Interferon-induced guanylate binding protein-1 (GBP-1) mediates an antiviral effect against vesicular stomatitis virus and encephalomyocarditis virus. *Virology* 256:8-14. 10.1006/viro.1999.9614

Ashkenazy H, Abadi S, Martz E, Chay O, Mayrose I, Pupko T, and Ben-Tal N. 2016. ConSurf 2016: an improved methodology to estimate and visualize evolutionary conservation in macromolecules. *Nucleic Acids Res* 44:W344-350. 10.1093/nar/gkw408

Ban T, Heymann JA, Song Z, Hinshaw JE, and Chan DC. 2010. OPA1 disease alleles causing dominant optic atrophy have defects in cardiolipin-stimulated GTP hydrolysis and

membrane tubulation. *Hum Mol Genet* 19:2113-2122. 10.1093/hmg/ddq088

Ban T, Ishihara T, Kohno H, Saita S, Ichimura A, Maenaka K, Oka T, Mihara K, and Ishihara N. 2017. Molecular basis of selective mitochondrial fusion by heterotypic action between OPA1 and cardiolipin. *Nat Cell Biol* 19:856-863. 10.1038/ncb3560

Baspinar A, Cukuroglu E, Nussinov R, Keskin O, and Gursoy A. 2014. PRISM: a web server and repository for prediction of protein-protein interactions and modeling their 3D complexes. *Nucleic Acids Res* 42:W285-289. 10.1093/nar/gku397

Belenguer P, and Pellegrini L. 2013. The dynamin GTPase OPA1: more than mitochondria? *Biochim Biophys Acta* 1833:176-183. 10.1016/j.bbamcr.2012.08.004

Bjellqvist B, Hughes GJ, Pasquali C, Paquet N, Ravier F, Sanchez JC, Frutiger S, and Hochstrasser D. 1993. The focusing positions of polypeptides in immobilized pH gradients can be predicted from their amino acid sequences. *Electrophoresis* 14:1023-1031.

Cao YL, Meng S, Chen Y, Feng JX, Gu DD, Yu B, Li YJ, Yang JY, Liao S, Chan DC, and Gao S. 2017. MFN1 structures reveal nucleotide-triggered dimerization critical for mitochondrial fusion. *Nature* 542:372-376. 10.1038/nature21077

Carelli V, Musumeci O, Caporali L, Zanna C, La Morgia C, Del Dotto V, Porcelli AM, Rugolo M, Valentino ML, Iommarini L, Maresca A, Barboni P, Carbonelli M, Trombetta C, Valente EM, Patergnani S, Giorgi C, Pinton P, Rizzo G, Tonon C, Lodi R, Avoni P,

388 Liguori R, Baruzzi A, Toscano A, and Zeviani M. 2015. Syndromic parkinsonism and
389 dementia associated with OPA1 missense mutations. *Ann Neurol* 78:21-38.
390 10.1002/ana.24410

391 Chan DC. 2012. Fusion and fission: interlinked processes critical for mitochondrial health. *Annu*
392 *Rev Genet* 46:265-287. 10.1146/annurev-genet-110410-132529

393 Chen H, Vermulst M, Wang YE, Chomyn A, Prolla TA, McCaffery JM, and Chan DC. 2010.
394 Mitochondrial fusion is required for mtDNA stability in skeletal muscle and tolerance of
395 mtDNA mutations. *Cell* 141:280-289. 10.1016/j.cell.2010.02.026

396 Cogliati S, Frezza C, Soriano ME, Varanita T, Quintana-Cabrera R, Corrado M, Cipolat S, Costa
397 V, Casarin A, Gomes LC, Perales-Clemente E, Salviati L, Fernandez-Silva P, Enriquez
398 JA, and Scorrano L. 2013. Mitochondrial cristae shape determines respiratory chain
399 supercomplexes assembly and respiratory efficiency. *Cell* 155:160-171.
400 10.1016/j.cell.2013.08.032

401 Crooks GE, Hon G, Chandonia JM, and Brenner SE. 2004. WebLogo: a sequence logo generator.
402 *Genome Res* 14:1188-1190. 10.1101/gr.849004

403 Del Dotto V, Fogazza M, Carelli V, Rugolo M, and Zanna C. 2018a. Eight human OPA1
404 isoforms, long and short: What are they for? *Biochim Biophys Acta Bioenerg* 1859:263-
405 269. 10.1016/j.bbabio.2018.01.005

406 Del Dotto V, Fogazza M, Lenaers G, Rugolo M, Carelli V, and Zanna C. 2018b. OPA1: How

much do we know to approach therapy? *Pharmacol Res* 131:199-210. 10.1016/j.phrs.2018.02.018

Del Dotto V, Mishra P, Vidoni S, Fogazza M, Maresca A, Caporali L, McCaffery JM, Cappelletti M, Baruffini E, Lenaers G, Chan D, Rugolo M, Carelli V, and Zanna C. 2017. OPA1 Isoforms in the Hierarchical Organization of Mitochondrial Functions. *Cell Rep* 19:2557-2571. 10.1016/j.celrep.2017.05.073

Eisner V, Picard M, and Hajnoczky G. 2018. Mitochondrial dynamics in adaptive and maladaptive cellular stress responses. *Nat Cell Biol* 20:755-765. 10.1038/s41556-018-0133-0

Elachouri G, Vidoni S, Zanna C, Pattyn A, Boukhaddaoui H, Gaget K, Yu-Wai-Man P, Gasparre G, Sarzi E, Delettre C, Olichon A, Loiseau D, Reynier P, Chinnery PF, Rotig A, Carelli V, Hamel CP, Rugolo M, and Lenaers G. 2011. OPA1 links human mitochondrial genome maintenance to mtDNA replication and distribution. *Genome Res* 21:12-20. 10.1101/gr.108696.110

Frezza C, Cipolat S, Martins de Brito O, Micaroni M, Beznoussenko GV, Rudka T, Bartoli D, Polishuck RS, Danial NN, De Strooper B, and Scorrano L. 2006. OPA1 controls apoptotic cristae remodeling independently from mitochondrial fusion. *Cell* 126:177-189. 10.1016/j.cell.2006.06.025

Haller O, Arnheiter H, Gresser I, and Lindenmann J. 1981. Virus-specific interferon action.

426 Protection of newborn Mx carriers against lethal infection with influenza virus. *J Exp*
427 *Med* 154:199-203.

428 Ishihara N, Fujita Y, Oka T, and Mihara K. 2006. Regulation of mitochondrial morphology
429 through proteolytic cleavage of OPA1. *EMBO J* 25:2966-2977.
430 10.1038/sj.emboj.7601184

431 Jimah JR, and Hinshaw JE. 2019. Structural Insights into the Mechanism of Dynamin
432 Superfamily Proteins. *Trends Cell Biol* 29:257-273. 10.1016/j.tcb.2018.11.003

433 Katoh K, and Standley DM. 2013. MAFFT multiple sequence alignment software version 7:
434 improvements in performance and usability. *Mol Biol Evol* 30:772-780.
435 10.1093/molbev/mst010

436 Kumar S, Stecher G, and Tamura K. 2016. MEGA7: Molecular Evolutionary Genetics Analysis
437 Version 7.0 for Bigger Datasets. *Mol Biol Evol* 33:1870-1874. 10.1093/molbev/msw054

438 Labbe K, Murley A, and Nunnari J. 2014. Determinants and functions of mitochondrial behavior.
439 *Annu Rev Cell Dev Biol* 30:357-391. 10.1146/annurev-cellbio-101011-155756

440 Laskowski RA, MacArthur MW, Moss DS, and Thornton JM. 1993. PROCHECK: a program to
441 check the stereochemical quality of protein structures. *Journal of applied crystallography*
442 26:283-291.

443 Lenaers G, Hamel C, Delettre C, Amati-Bonneau P, Procaccio V, Bonneau D, Reynier P, and
444 Milea D. 2012. Dominant optic atrophy. *Orphanet J Rare Dis* 7:46. 10.1186/1750-1172-

445 7-46

446 Liu R, and Chan DC. 2017. OPA1 and cardiolipin team up for mitochondrial fusion. *Nat Cell*
447 *Biol* 19:760-762. 10.1038/ncb3565

448 MacVicar T, and Langer T. 2016. OPA1 processing in cell death and disease - the long and short
449 of it. *J Cell Sci* 129:2297-2306. 10.1242/jcs.159186

450 Marelli C, Amati-Bonneau P, Reynier P, Layet V, Layet A, Stevanin G, Brissaud E, Bonneau D,
451 Durr A, and Brice A. 2011. Heterozygous OPA1 mutations in Behr syndrome. *Brain*
452 134:e169; author reply e170. 10.1093/brain/awq306

453 Noguchi M, and Kasahara A. 2018. Mitochondrial dynamics coordinate cell differentiation.
454 *Biochem Biophys Res Commun* 500:59-64. 10.1016/j.bbrc.2017.06.094

455 O'Leary NA, Wright MW, Brister JR, Ciufo S, Haddad D, McVeigh R, Rajput B, Robbertse B,
456 Smith-White B, Ako-Adjei D, Astashyn A, Badretdin A, Bao Y, Blinkova O, Brover V,
457 Chetvernin V, Choi J, Cox E, Ermolaeva O, Farrell CM, Goldfarb T, Gupta T, Haft D,
458 Hatcher E, Hlavina W, Joardar VS, Kodali VK, Li W, Maglott D, Masterson P,
459 McGarvey KM, Murphy MR, O'Neill K, Pujar S, Rangwala SH, Rausch D, Riddick LD,
460 Schoch C, Shkeda A, Storz SS, Sun H, Thibaud-Nissen F, Tolstoy I, Tully RE, Vatsan
461 AR, Wallin C, Webb D, Wu W, Landrum MJ, Kimchi A, Tatusova T, DiCuccio M, Kitts
462 P, Murphy TD, and Pruitt KD. 2016. Reference sequence (RefSeq) database at NCBI:
463 current status, taxonomic expansion, and functional annotation. *Nucleic Acids Res*

44:D733-745. 10.1093/nar/gkv1189

Olichon A, Baricault L, Gas N, Guillou E, Valette A, Belenguer P, and Lenaers G. 2003. Loss of OPA1 perturbates the mitochondrial inner membrane structure and integrity, leading to cytochrome c release and apoptosis. *J Biol Chem* 278:7743-7746. 10.1074/jbc.C200677200

Patten DA, Wong J, Khacho M, Soubannier V, Mailloux RJ, Pilon-Larose K, MacLaurin JG, Park DS, McBride HM, Trinkle-Mulcahy L, Harper ME, Germain M, and Slack RS. 2014. OPA1-dependent cristae modulation is essential for cellular adaptation to metabolic demand. *EMBO J* 33:2676-2691. 10.15252/embj.201488349

Pernas L, and Scorrano L. 2016. Mito-Morphosis: Mitochondrial Fusion, Fission, and Cristae Remodeling as Key Mediators of Cellular Function. *Annu Rev Physiol* 78:505-531. 10.1146/annurev-physiol-021115-105011

Praefcke GJ, and McMahon HT. 2004. The dynamin superfamily: universal membrane tubulation and fission molecules? *Nat Rev Mol Cell Biol* 5:133-147. 10.1038/nrm1313

Rose PW, Prlic A, Altunkaya A, Bi C, Bradley AR, Christie CH, Costanzo LD, Duarte JM, Dutta S, Feng Z, Green RK, Goodsell DS, Hudson B, Kalro T, Lowe R, Peisach E, Randle C, Rose AS, Shao C, Tao YP, Valasatava Y, Voigt M, Westbrook JD, Woo J, Yang H, Young JY, Zardecki C, Berman HM, and Burley SK. 2017. The RCSB protein data bank: integrative view of protein, gene and 3D structural information. *Nucleic Acids Res*

45:D271-D281. 10.1093/nar/gkw1000

Simpson RJ. 2006. SDS-PAGE of Proteins. *CSH Protoc* 2006. 10.1101/pdb.prot4313

Song Z, Chen H, Fiket M, Alexander C, and Chan DC. 2007. OPA1 processing controls mitochondrial fusion and is regulated by mRNA splicing, membrane potential, and Yme1L. *J Cell Biol* 178:749-755. 10.1083/jcb.200704110

Song Z, Ghochani M, McCaffery JM, Frey TG, and Chan DC. 2009. Mitofusins and OPA1 mediate sequential steps in mitochondrial membrane fusion. *Mol Biol Cell* 20:3525-3532. 10.1091/mbc.E09-03-0252

van der Bliek AM, Shen Q, and Kawajiri S. 2013. Mechanisms of mitochondrial fission and fusion. *Cold Spring Harb Perspect Biol* 5. 10.1101/cshperspect.a011072

Wai T, and Langer T. 2016. Mitochondrial Dynamics and Metabolic Regulation. *Trends Endocrinol Metab* 27:105-117. 10.1016/j.tem.2015.12.001

Wittig I, Braun HP, and Schagger H. 2006. Blue native PAGE. *Nat Protoc* 1:418-428. 10.1038/nprot.2006.62

Xu J, and Zhang Y. 2010. How significant is a protein structure similarity with TM-score = 0.5? *Bioinformatics* 26:889-895. 10.1093/bioinformatics/btq066

Yamaguchi R, Lartigue L, Perkins G, Scott RT, Dixit A, Kushnareva Y, Kuwana T, Ellisman MH, and Newmeyer DD. 2008. Opa1-mediated cristae opening is Bax/Bak and BH3 dependent, required for apoptosis, and independent of Bak oligomerization. *Mol Cell*

31:557-569. 10.1016/j.molcel.2008.07.010

Yang J, Yan R, Roy A, Xu D, Poisson J, and Zhang Y. 2015. The I-TASSER Suite: protein structure and function prediction. *Nat Methods* 12:7-8. 10.1038/nmeth.3213

Yu-Wai-Man P, Griffiths PG, Gorman GS, Lourenco CM, Wright AF, Auer-Grumbach M, Toscano A, Musumeci O, Valentino ML, Caporali L, Lamperti C, Tallaksen CM, Duffey P, Miller J, Whittaker RG, Baker MR, Jackson MJ, Clarke MP, Dhillon B, Czermin B, Stewart JD, Hudson G, Reynier P, Bonneau D, Marques W, Jr., Lenaers G, McFarland R, Taylor RW, Turnbull DM, Votruba M, Zeviani M, Carelli V, Bindoff LA, Horvath R, Amati-Bonneau P, and Chinnery PF. 2010. Multi-system neurological disease is common in patients with OPA1 mutations. *Brain* 133:771-786. 10.1093/brain/awq007

Zanna C, Ghelli A, Porcelli AM, Karbowski M, Youle RJ, Schimpf S, Wissinger B, Pinti M, Cossarizza A, Vidoni S, Valentino ML, Rugolo M, and Carelli V. 2008. OPA1 mutations associated with dominant optic atrophy impair oxidative phosphorylation and mitochondrial fusion. *Brain* 131:352-367. 10.1093/brain/awm335

Zerbino DR, Achuthan P, Akanni W, Amode MR, Barrell D, Bhai J, Billis K, Cummins C, Gall A, Giron CG, Gil L, Gordon L, Haggerty L, Haskell E, Hourlier T, Izuogu OG, Janacek SH, Juettemann T, To JK, Laird MR, Lavidas I, Liu Z, Loveland JE, Maurel T, McLaren W, Moore B, Mudge J, Murphy DN, Newman V, Nuhn M, Ogeh D, Ong CK, Parker A, Patricio M, Riat HS, Schuilenburg H, Sheppard D, Sparrow H, Taylor K, Thormann A, Vullo A, Walts B, Zadissa A, Frankish A, Hunt SE, Kostadima M, Langridge N, Martin

522 FJ, Muffato M, Perry E, Ruffier M, Staines DM, Trevanion SJ, Aken BL, Cunningham F,
523 Yates A, and Flicek P. 2018. Ensembl 2018. *Nucleic Acids Res* 46:D754-D761.
524 10.1093/nar/gkx1098

525 Zhang J, Liang Y, and Zhang Y. 2011. Atomic-Level Protein Structure Refinement Using
526 Fragment-Guided Molecular Dynamics Conformation Sampling. *Structure* 19:1784-1795.
527 10.1016/j.str.2011.09.022

528 Zhang Y, and Skolnick J. 2005. TM-align: a protein structure alignment algorithm based on the
529 TM-score. *Nucleic Acids Res* 33:2302-2309. 10.1093/nar/gki524

530

Figure Legends

Figure 1: Schematic representation of human OPA1 isoforms. (A) In human, *OPA1* gene is built from 30 exons, 3 of which (4, 4b and 5b) are alternatively spliced leading to 8 variants (isoforms 1-8). OPA1 exons (numbers) were schematized by short-term. Mitochondrial proteolytic cleavage sites for mitochondrial processing peptidase (MPP), OMA1 (S1) and YME1L (S2) were indicated. (B) Average hydropathicity of OPA1 N-terminal exon-encoded peptides. (C) The pI value of OPA1 N-terminal exon-encoded peptides. Proteolytic cleavage at S1 and S2 sites by the OMA1 and YME1L peptidase generates the IMS soluble s-forms. Exon 5-encoded peptide was divided into two parts by site S1, while the N-terminal part was labeled with 5^N and the C-terminal was labeled with 5^C. The same labeling method was used for exon 5b-encoded peptide cleaved at site S2.

Figure 2: The three-dimensional structure of human OPA1 protein. (A) Structure-based domain architecture of OPA1 isoform 8. The domain assignment was indicated below. Each domain was labeled by different colors, corresponding to the schematic representation of exons. (B) Modeled structure of isoform 8 excluding MTS and TM (long form). It was showed in a cartoon mode. The N-terminal region was rich in alpha helix and did not include specific domains, while The C-terminal region of OPA1 protein was a dense structure containing multiple domains. (C) Modeled structure of human OPA1 protein (short form). It was displayed in a cartoon mode.

Figure 3: Comparison between the structure of OPA1 protein and other human dynamins. (A) Phylogenetic tree of human dynamin superfamily members. The structure of OPA1 protein was compared with that of dynamin 1 (B), dynamin 3 (C), Drp1 (D), MxA (E), MxB (F), mitofusin 1 (G), GBP1 (H), atlastin 1 (I) and atlastin 3 (J) separately. Phylogenetic analyses were conducted by the bootstrap neighbor joining method. The tree was drawn to scale, with branch lengths in the same units as those of the evolutionary distances used to infer the phylogenetic tree. The structure of OPA1 was showed by modeled structure, while dynamin 1, dynamin 3, Drp1, MxA, MxB, mitofusin 1, GBP1, atlastin 1 and atlastin 3 were displayed by crystal structures (PDB code: 3snh, 5a3f, 4bej, 3szr, 4whj, 5yew, 1dg3, 3q5e and 5vgr). The TM-score calculated according to the comparison results was also displayed.

Figure 4: Prediction of OPA1 homodimeric interaction. (A) One stable mode of dimerization. The homodimerization interface had been rotated. (B) The other possible mode of dimerization. Cartoon figure of OPA1 homodimeric interaction predicted through docking calculations. The right was inter-residues interaction in potential dimerization interfaces. The interaction partners were connected by broken lines. The modeled structure of OPA1 C-terminal region was used for docking analysis. The residues were numbered according to the human OPA1 isoform 8.

Figure 5: Evolutionary conservation of vertebrates OPA1 protein sequence. (A) Mapping of evolutionary conservation of amino acid positions in the OPA1. The conservation scale was defined from the most variable amino acid positions (grade 1, colored turquoise) which were considered as rapidly evolving, to the most conservative positions (grade 9, colored maroon)

570 which were considered as slowly evolving. The nine-color conservation grades were mapped
571 onto the structure of human OPA1. (B) Distribution of evolutionary conservation in human
572 OPA1 gene according to the exons. The highest percent of maroon represented the most
573 conserved position in a protein.

Figure 1

Figure 1: Schematic representation of human OPA1 isoforms.

(A) In human, *OPA1* gene is built from 30 exons, 3 of which (4, 4b and 5b) are alternatively spliced leading to 8 variants (isoforms 1-8). OPA1 exons (numbers) were schematized by short-term. Mitochondrial proteolytic cleavage sites for mitochondrial processing peptidase (MPP), OMA1 (S1) and YME1L (S2) were indicated. (B) Average hydropathicity of OPA1 N-terminal exon-encoded peptides. (C) The pI value of OPA1 N-terminal exon-encoded peptides. Proteolytic cleavage at S1 and S2 sites by the OMA1 and YME1L peptidase generates the IMS soluble s-forms. Exon 5-encoded peptide was divided into two parts by site S1, while the N-terminal part was labeled with 5^{N} and the C-terminal was labeled with 5^{C}. The same labeling method was used for exon 5b-encoded peptide cleaved at site S2.

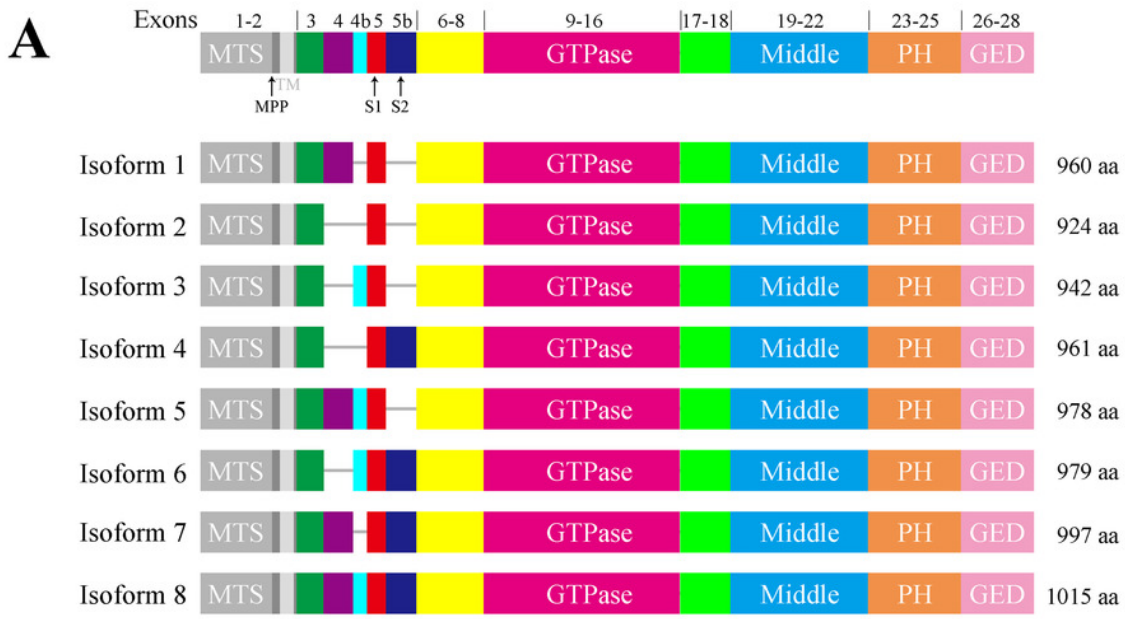
A
Exons
1-2
3
4
4b
5
5b
6-8
9-16
17-18
19-22
23-25
26-28
MTS
GTPase
Middle
PH
GED
TM
MPP
S1
S2
Isoform 1
960 aa
Isoform 2
924 aa
Isoform 3
942 aa
Isoform 4
961 aa
Isoform 5
978 aa
Isoform 6
979 aa
Isoform 7
997 aa
Isoform 8
1015 aa

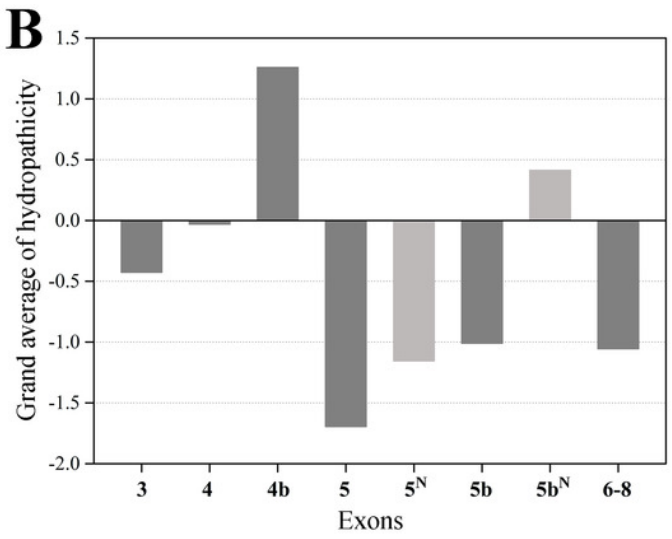
B
Grand average of hydropathicity
1.5
1.0
0.5
0.0
-0.5
-1.0
-1.5
-2.0
3
4
4b
5
5N
5b
5bN
6-8
Exons

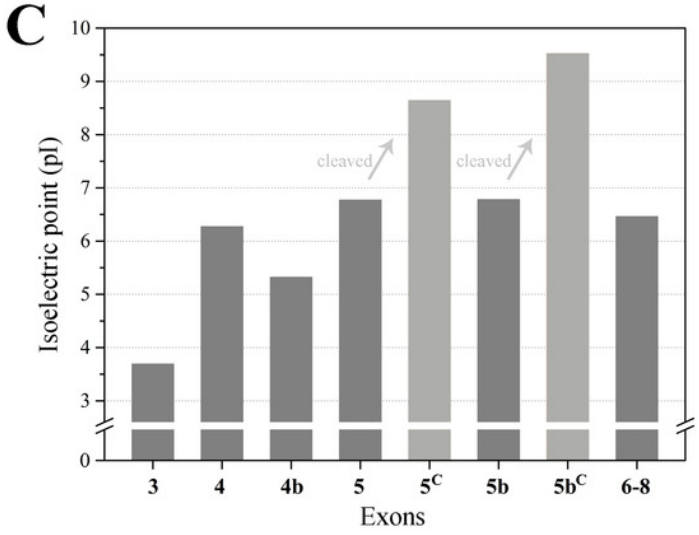
C
Isoelectric point (pI)
10
9
8
7
6
5
4
3
0
cleaved
cleaved
3
4
4b
5
5C
5b
5bC
6-8
Exons

Figure 2

Figure 2: The three-dimensional structure of human OPA1 protein.

(A) Structure-based domain architecture of OPA1 isoform 8. The domain assignment was indicated below. Each domain was labeled by different colors, corresponding to the schematic representation of exons. (B) Modeled structure of isoform 8 excluding MTS and TM (long form). It was showed in a cartoon mode. The N-terminal region was rich in alpha helix and did not include specific domains, while The C-terminal region of OPA1 protein was a dense structure containing multiple domains. (C) Modeled structure of human OPA1 protein (short form). It was displayed in a cartoon mode.

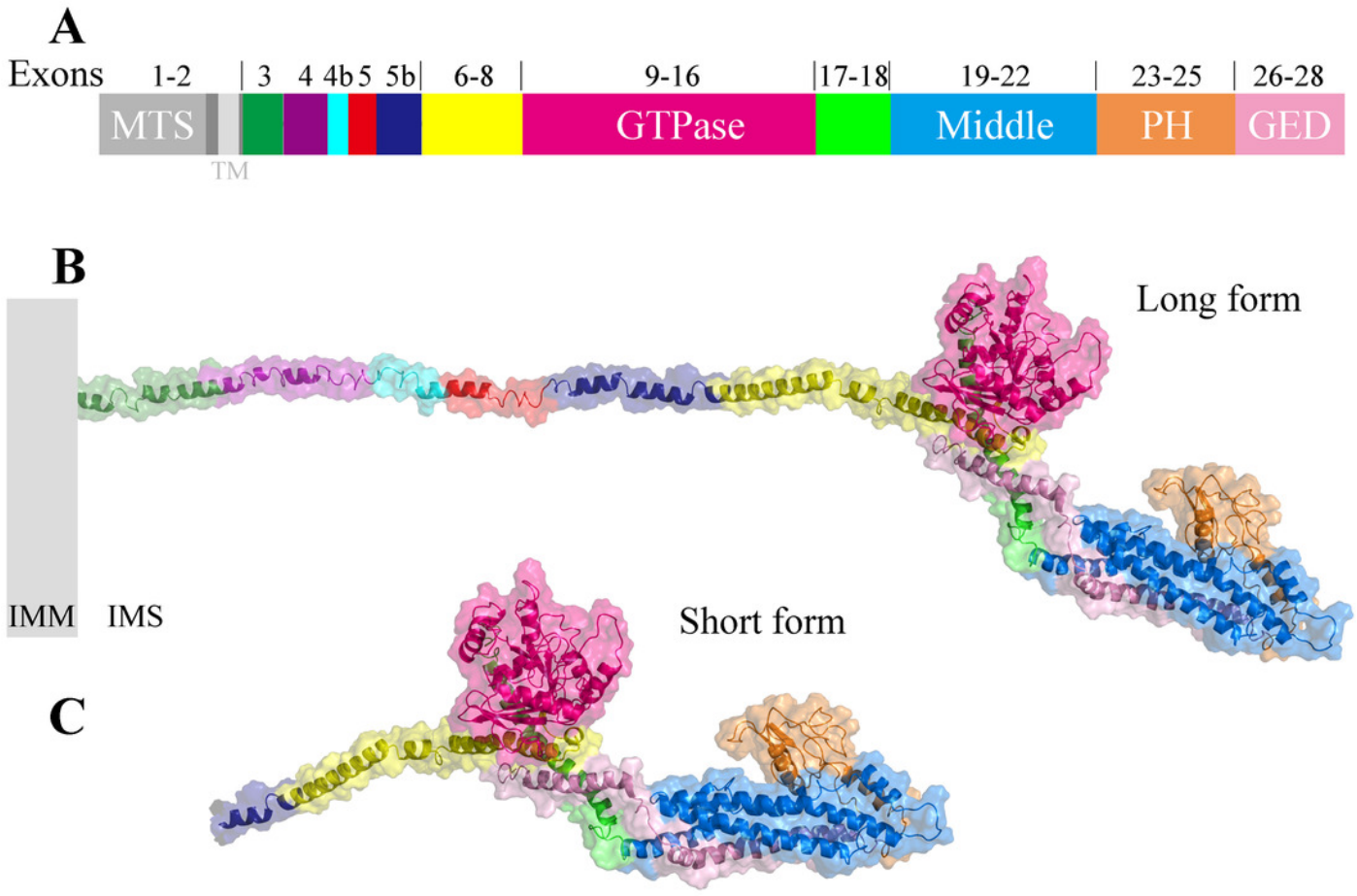

Figure 3

Figure 3: Comparison between the structure of OPA1 protein and other human dynamins.

(A) Phylogenetic tree of human dynamin superfamily members. The structure of OPA1 protein was compared with that of dynamin 1 (B), dynamin 3 (C), Drp1 (D), MxA (E), MxB (F), mitofusin 1 (G), GBP1 (H), atlastin 1 (I) and atlastin 3 (J) separately. Phylogenetic analyses were conducted by the bootstrap neighbor joining method. The tree was drawn to scale, with branch lengths in the same units as those of the evolutionary distances used to infer the phylogenetic tree. The structure of OPA1 was showed by modeled structure, while dynamin 1, dynamin 3, Drp1, MxA, MxB, mitofusin 1, GBP1, atlastin 1 and atlastin 3 were displayed by crystal structures (PDB code: 3snh, 5a3f, 4bej, 3szr, 4whj, 5yew, 1dg3, 3q5e and 5vgr). The TM-score calculated according to the comparison results was also displayed.

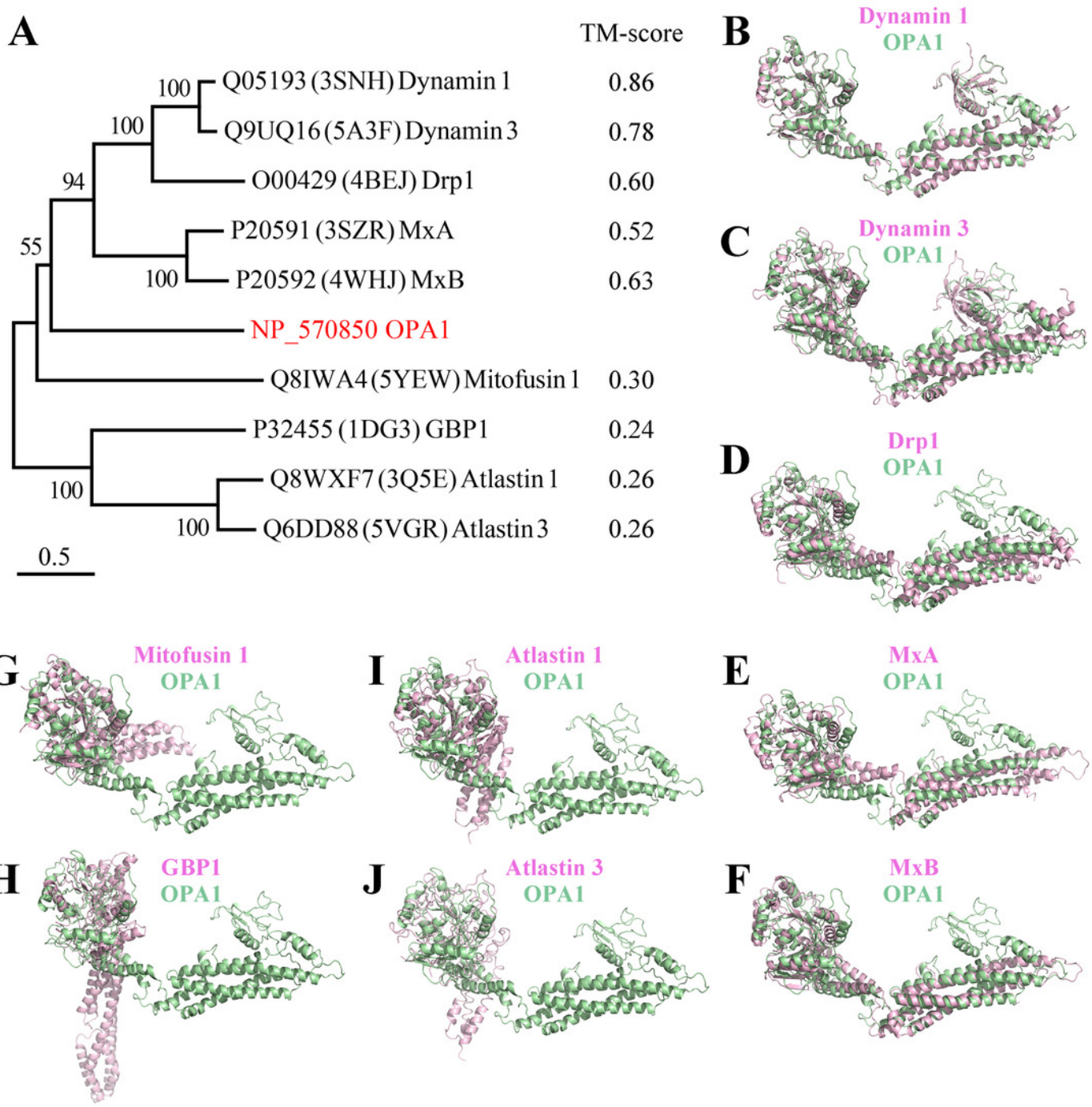
A
TM-score
100
Q05193 (3SNH) Dynamin 1
0.86
100
Q9UQ16 (5A3F) Dynamin 3
0.78
94
O00429 (4BEJ) Drp1
0.60
P20591 (3SZR) MxA
0.52
55
100
P20592 (4WHJ) MxB
0.63
NP_570850 OPA1
Q8IWA4 (5YEW) Mitofusin 1
0.30
P32455 (1DG3) GBP1
0.24
100
Q8WXF7 (3Q5E) Atlastin 1
0.26
100
Q6DD88 (5VGR) Atlastin 3
0.26
0.5
B
Dynamin 1
OPA1
C
Dynamin 3
OPA1
D
Drp1
OPA1
G
Mitofusin 1
OPA1
I
Atlastin 1
OPA1
E
MxA
OPA1
H
GBP1
OPA1
J
Atlastin 3
OPA1
F
MxB
OPA1

Figure 4

Figure 4: Prediction of OPA1 homodimeric interaction.

(A) One stable mode of dimerization. The homodimerization interface had been rotated. (B) The other possible mode of dimerization. Cartoon figure of OPA1 homodimeric interaction predicted through docking calculations. The right was inter-residues interaction in potential dimerization interfaces. The interaction partners were connected by broken lines. The modeled structure of OPA1 C-terminal region was used for docking analysis. The residues were numbered according to the human OPA1 isoform 8. "

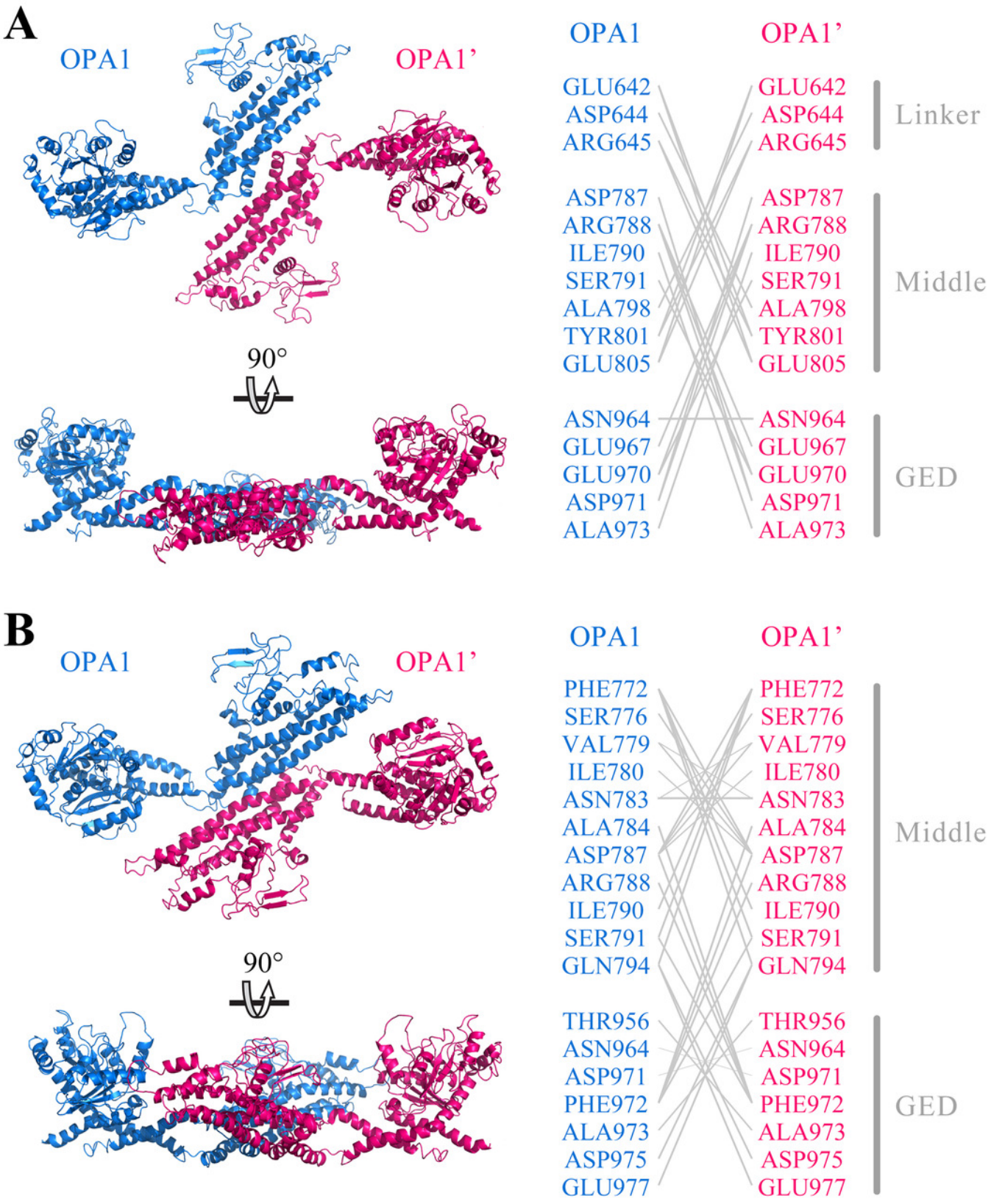
A
OPA1
OPA1'
90°
OPA1
OPA1'
GLU642
ASP644
ARG645
ASP787
ARG788
ILE790
SER791
ALA798
TYR801
GLU805
ASN964
GLU967
GLU970
ASP971
ALA973
Linker
Middle
GED
B
OPA1
OPA1'
90°
OPA1
OPA1'
PHE772
SER776
VAL779
ILE780
ASN783
ALA784
ASP787
ARG788
ILE790
SER791
GLN794
THR956
ASN964
ASP971
PHE972
ALA973
ASP975
GLU977
Middle
GED

Figure 5

Figure 5: Evolutionary conservation of vertebrates OPA1 protein sequence.

(A) Mapping of evolutionary conservation of amino acid positions in the OPA1. The conservation scale was defined from the most variable amino acid positions (grade 1, colored turquoise) which were considered as rapidly evolving, to the most conservative positions (grade 9, colored maroon) which were considered as slowly evolving. The nine-color conservation grades were mapped onto the structure of human OPA1. (B) Distribution of evolutionary conservation in human OPA1 gene according to the exons. The highest percent of maroon represented the most conserved position in a protein.

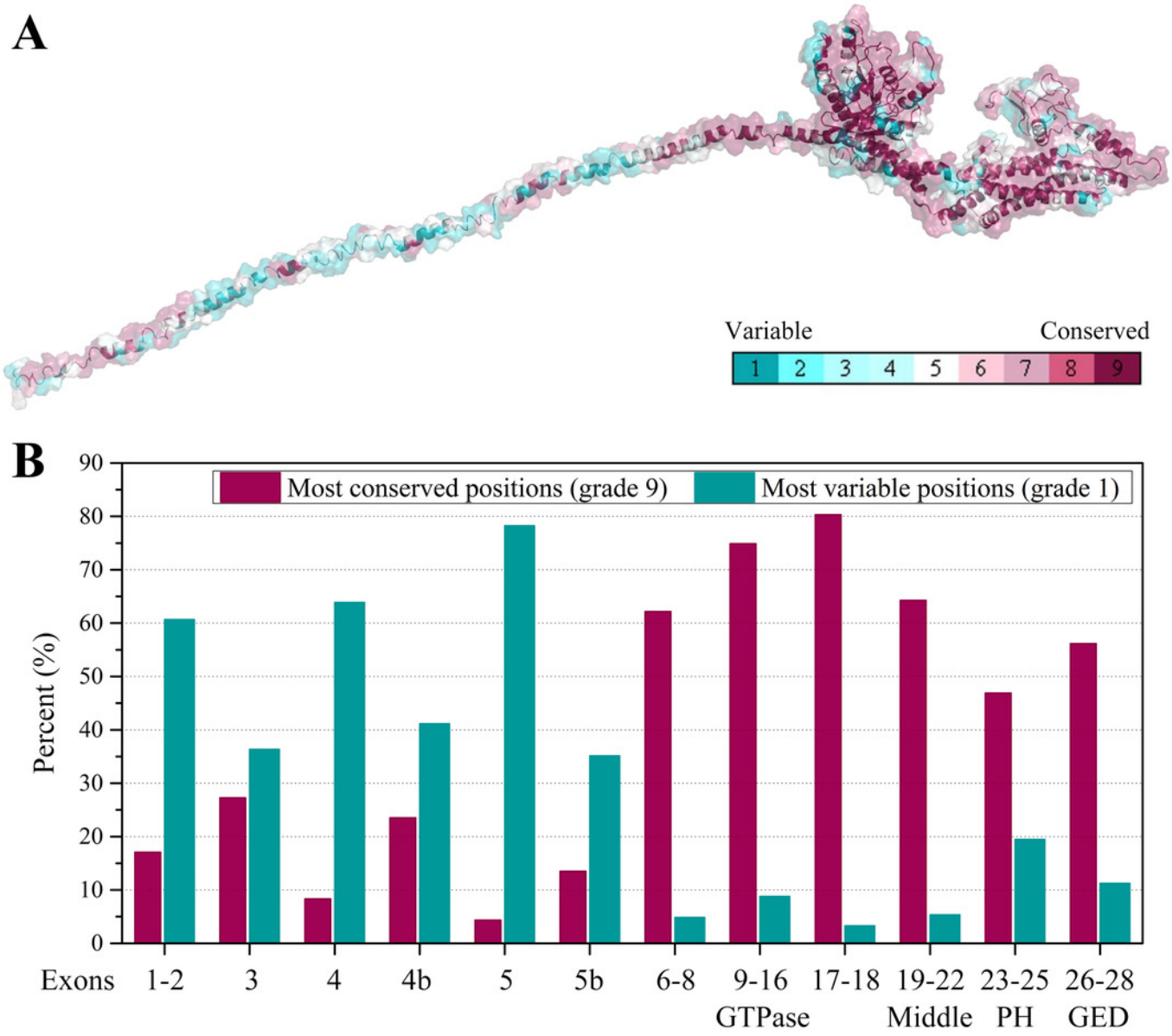
A
Variable
Conserved
1 2 3 4 5 6 7 8 9
B
Most conserved positions (grade 9)
Most variable positions (grade 1)
Percent (%)
0 10 20 30 40 50 60 70 80 90
Exons
1-2 3 4 4b 5 5b 6-8 9-16 17-18 19-22 23-25 26-28
GTPase
Middle
PH
GED